Kinetic modeling of lag times during photo-induced disinfection of E. coli in sunlit surface waters: Unraveling the pathways of exogenous inactivation.

(Article begins on next page)

05 November 2024

Kinetic modeling of lag times during photo-induced disinfection of *E. coli* in sunlit surface waters: Unraveling the pathways of exogenous inactivation.

Efraim A. Serna-Galvis[a,b], Jean Arnaud Troyon[a], Stefanos Giannakis[a], Ricardo A. Torres-Palma[b], Luca Carena[c], Davide Vione[c,*], Cesar Pulgarin[a,**]

[a] *School of Basic Sciences (SB), Institute of Chemical Science and Engineering (ISIC), Group of Advanced Oxidation Processes (GPAO), École Polytechnique Fédérale de Lausanne (EPFL), Station 6, CH-1015 Lausanne, Switzerland*

[b] *Grupo de Investigación en Remediación Ambiental y Biocatálisis (GIRAB), Instituto de Química, Facultad de Ciencias Exactas y Naturales, Universidad de Antioquía UdeA, Calle 70 No. 52-21, Medellín, Colombia*

[c] *Dipartimento di Chimica, Università di Torino, Via P. Giuria 5, 10125, Torino, Italy*

* Corresponding Author: Prof. Dr. Davide Vione, E-mail: davide.vione@unito.it

** Corresponding Author: Prof. Dr. Cesar Pulgarin, E-mail: cesar.pulgarin@epfl.ch

Abstract

The present work presents a kinetic analysis of the exogenous photo-induced disinfection of *E. coli* in natural waters. Herein, the inactivation of bacteria by light and photo-generated transient species, i.e., hydroxyl radical (HO$^\bullet$), excited triplet states of organic matter (^{3}CDOM*) and singlet oxygen (^{1}O$_2$), was studied. It was found that the exogenous disinfection of *E. coli* proceeds through a lag time, followed by an exponential phase triggered by photo-generated HO$^\bullet$, ^{1}O$_2$ and ^{3}CDOM*. Also,

we report that the concentration increase of transient species (and especially HO$^{\bullet}$) precursors decreased the lag times of bacteria inactivation. Due to the limitations of the competition kinetics methodology to include the lag phase, an alternative strategy to study the interaction between *E. coli* and photo-generated transient species was proposed, considering the log-linear pseudo-first order rate constants and lag-times. On this basis and by using APEX software, a full kinetic analysis of exogenous bacterial inactivation, taking into account both lag-time and exponential decay, was developed. This approach provided insights into the conditions that could make exogenous inactivation competitive with the endogenous process for the *E. coli* inactivation in natural sunlit waters. Hence, this research contributes to the understanding of fundamental kinetic aspects of photoinduced bacterial inactivation, which is the basis for light-assisted processes such as the solar disinfection (SODIS).

1. Introduction

Solar irradiation of natural waters is an efficient means of disinfection, especially against microorganisms such as *Escherichia coli, Enterococcus fecalis, Vibrio cholerae* or *Salmonella sp.,* which are responsible for several enteric diseases (McGuigan et al., 2012). Indeed, solar light inactivates bacteria in natural waters and it has been developed into a technique broadly known as SODIS, which is successfully used in many developing countries in order to obtain safe drinking water (Fernàndez-Ibañez et al., 2017; Ndounla et al., 2014). Contrary to its simple application, solar-mediated bacterial inactivation is a complex process that involves a range of diverse intracellular oxidative pathways (Giannakis et al., 2016), as well as extracellular attacks by Reactive Oxygen Species (ROS, such as hydroxyl radical and singlet oxygen) or other transient species produced in the water bulk or inside the cell (Davies-Colley et al., 2000; Maraccini et al., 2016; Nelson et al., 2018).

Natural waters contain compounds that can act as photosensitizers, e.g., Chromophoric Dissolved Organic Mater (CDOM), nitrate or nitrite. The photosensitizers absorb sunlight and produce a range of reactive transient species. For instance, the interaction of solar light with CDOM, nitrate and nitrite yields hydroxyl radical (HO•) (Vione et al., 2006). Furthermore, CDOM can also induce the generation of other species of interest for bacterial inactivation, namely singlet oxygen ($^1O_2$) and excited triplet states of organic matter ($^3CDOM^*$) (Rosario-Ortiz and Canonica, 2016).

A way to describe the interaction of bacteria with photogenerated transient species (i.e., HO•, $^3CDOM^*$, $^1O_2$) is kinetic analysis based on second-order reaction rate constants (Serna-Galvis et al., 2018; Spuhler et al., 2010), which is currently used in the case of xenobiotics (Minella et al., 2017) and can also be applied to viruses (Kohn et al., 2016). For chemical contaminants, two different methodologies are mostly used to determine the second-order reaction rate constants with photo-induced transients, and they could be considered for bacterial inactivation as well. The first method uses probe compounds to determine the steady-state concentration or the formation rate of each

transient species, or scavengers that selectively react with the transients and inhibit the relevant degradation processes (De Laurentiis et al., 2014). The second method is based on competition kinetics, which uses reference compounds of known reactivity with the transients and compares their degradation kinetics with that of the target xenobiotic (Onstein et al., 1999). In the case of bacteria, the former method may prove difficult to use as the probe compounds and the scavengers (which are commonly alcohols or aromatic derivatives) and/or their degradation products have toxic effect on living cells (see Text S1 and Figure S1 in the Supplementary Material, hereafter SM). Meanwhile, competition kinetics was recently proven to be a viable option in the case of bacteria, provided that non-toxic reference compounds are chosen, and abetted to determine the second-order reaction rate constants of transient species with bacteria (Serna-Galvis et al., 2018) or viruses (Kohn et al., 2016). However, these rate constants can only be measured in the exponential decay phase that follows the lag phase in bacterial inactivation (Serna-Galvis et al., 2018).

In many cases, bacterial disinfection promoted by sunlight is characterized by an initial lag time followed by an exponential decay (Giannakis et al., 2018; Giannakis et al., 2015; Ndounla et al., 2014, 2013; Sciacca et al., 2010). The prevailing theory for the explanation of the phenomenon lies in the need for damages via an intracellular bacterial oxidative stress, and the capacity of bacteria to withstand a certain level of damage (demonstrated as lag), after which their capacity to maintain their life cycle is diminished (Giannakis et al., 2018; Imlay, 2003). Hence, a complete kinetic analysis for describing and modeling disinfection efficiencies and inactivation rates of bacteria in sunlight-exposed surface waters should include both lag phase and exponential decay.

This work presents an innovative strategy for the kinetic analysis of the lag time during the inactivation of bacteria promoted by photo-induced transient species. Initially, experimental results of photo-induced inactivation of *E. coli* in water, which show lag phase and exponential decay, are presented. After discussing the limitation of competition kinetics to include the lag phase of bacterial inactivation, an alternative kinetic analysis is hereby proposed. Then, we determined how

the photogenerated transients (i.e., HO•, $^3CDOM^*$ and $^1O_2$) affect both the lag times and the subsequent exponential inactivation of the bacteria. Finally, a deep kinetic analysis (by simulation with the APEX software (Bodrato and Vione, 2014)) of photo-induced bacterial inactivation is carried out by including the lag phase, under different conditions of water depth and matrix composition.

2 Materials and methods

2.1 Reagents

Sodium nitrate ($NaNO_3$, 99%), anthraquinone-2-sulfonate (AQ2S, 98%), rose bengal (RB), sodium chloride (NaCl, 99.5%), potassium chloride (KCl, 99%), plate count agar powder (PCA), acesulfame K (ACE, 99%), naproxen (NPX, 98%), aniline (99.5%), N,N-dimethyl aniline (DMA, 99%), furfuryl alcohol (FFA, 98%) and tetra-butyl ammonium hydrogen sulfate (TBA, ≥99%) were purchased from Sigma-Aldrich. Acetonitrile (ACN, ≥99.8%) was obtained from Avantor. 2-Propanol (IPA, 99%) was provided by Merck. All solutions were prepared using Milli-Q water obtained from a Millipore (Elix) Merck Instrument.

$NaNO_3$ was used as source of hydroxyl radicals (HO•) (Mack and Bolton, 1999). AQ2S was chosen as a proxy compound for CDOM, to assess the photochemical production of triplet states and their reactivity. AQ2S belongs to the class of quinones, which are significant photoactive components of dissolved organic matter (Cory and McKnight, 2005). When irradiated by UVA, AQ2S selectively produces $^3AQ2S^*$ without yielding either singlet oxygen or hydroxyl radicals (Loeff et al., 1984; Maddigapu et al., 2010). For this reason, in this work $^3AQ2S^*$ was used as $^3CDOM^*$ proxy. Because $^3AQ2S^*$ is known to be more reactive than typical $^3CDOM^*$ (Avetta et al., 2016), the associated reactivity is an upper limit for that of CDOM triplet states. Finally, Rose Bengal (RB)

was used as source of singlet oxygen ($^1O_2$), due to its high ability to generate this transient species (Kochevar and Redmond, 2000).

2.2 Microorganism preparation and bacterial enumeration

Escherichia coli K12 (*E. coli*) from the "Deutsche Sammlung von Mikroorganismen und Zellkulturen" (DSM No. 498) was used for the disinfection experiments. *E. coli* was selected as model bacterial species due to its common presence in fecal-contaminated waters. It is a simple prokaryotic microorganism, but it constitutes an adequate model for various types of enteric-related diseases (Giannakis, 2018). The bacteria were prepared in the same way as described in our previous works (Giannakis et al., 2015). In the reaction systems, the initial *E. coli* population was 10^6 CFU mL^{-1} and was obtained by dilution of the stock solution.

Samples of 1.0 mL were periodically taken from the reactor into sterile Eppendorf vials. Successive dilutions were made using a saline solution of 0.8% w/w NaCl and 0.08% w/w KCl, and 100 µL of these were plated on plate count agar and incubated (18-24 h at 37°C) before enumeration.

2.3 Irradiation experiments

Aqueous samples of 50 mL were introduced in cylindrical Pyrex glass bottles (diameter: 4 cm, height: 7.5 cm) with a cut-off wavelength of 295 nm. The solutions were magnetically stirred at 350 rpm. To ensure a selective excitation of the photosensitizers and minimize the occurrence of any unwanted side-photoreactions, specific lamps were used for each sensitization experiment. Three 20 W Philips TL-D 01 UVB lamps (40 W m^{-2} irradiance) with a narrowband emission at 313 nm were used to generate HO• from NaNO$_3$. Five 18 W Philips TL-D BLB lamps (68 W m^{-2}) with a narrowband emission at 365 nm were used to produce ^{3}AQ2S*. The excitation of RB as $^1O_2$ source was done under yellow light, using five Philips TL D 18 W/16 lamps (38 W m^{-2}). The irradiance

emitted by the lamps was measured using an USB2000+ spectrophotometer equipped with a pyranometer, which is able to measure irradiance from 300 to 2800 nm. The lamps were turned on 30 min before the beginning of the experiments, to ensure a constant irradiation as well as a constant wavelength emission.

2.4 Analytical procedures

The analysis of the different reference compounds used for competition kinetics, with the purpose of assessing their time evolution, was done by using a HP Agilent 1100 series HPLC equipped with a DAD detector and an Ascentis C18 HPLC column. The chromatographic methods are summarized in Table S1 in the SM.

2.5 Kinetic modeling of the photo-inactivation processes

The steady-state concentrations of photo-induced transient species (HO•, $^1O_2$, $^3CDOM^*$) in sunlit natural waters and the corresponding first-order rate constants of bacterial inactivation after the lag phase were modeled with the APEX software (Aquatic Photochemistry of Environmentally-occurring Xenobiotics), which is available for free as Electronic Supplementary Information of Bodrato and Vione (2014). APEX predicts photochemical reaction kinetics (in the case of bacteria, it predicts the exogenous photo-inactivation rate constants after the lag phase (Serna-Galvis et al., 2018)) from photo-reactivity parameters (in this case, the second-order inactivation rate constants of *E. coli* by HO•, $^1O_2$ and $^3CDOM^*$), sunlight irradiance, and data of water chemistry and depth (Bodrato and Vione, 2014). APEX calculates the absorption of radiation by the photosensitizers (CDOM, nitrate and nitrite) on the basis of competition for sunlight irradiance, in a Lambert-Beer approach (Bodrato and Vione, 2014; Braslavsky, 2007). The software considers both the kinetics of transient photo-generation by the irradiated photo-sensitizers, and the scavenging of the transients themselves by the system components. In particular, HO$^•$ is scavenged by DOM (dissolved organic

matter, of which CDOM is the light-absorbing fraction) as well as by HCO_3^- and CO_3^{2-}, $^1O_2$ is inactivated by collision with water molecules, and $^3CDOM^*$ is largely quenched by dissolved O_2 (Vione et al., 2014). The model results apply to well-mixed waters and provide average values over the whole water column, with contributions from the well-illuminated surface layer and from darker water in the lower depths (Loiselle et al., 2008). As mentioned, the software is suitable to model the exponential decay phase of exogenous bacterial photo-inactivation. In contrast, the modeling of the lag phase cannot be undertaken by using APEX alone.

3. Results and Discussion

3.1 The lag phase and exponential decay during *E. coli* disinfection by photo-induced transient species

The measured experimental data for the photo-induced of inactivation of *E. coli* are reported in Figure 1. This figure presents *E. coli* inactivation under irradiation in absence and presence of the transient species precursors (i.e., NaNO$_3$, AQ2S and RB). Two important aspects of the disinfection conditions have to be noted here: 1) the precursors did not affect the bacterial population after long periods of exposure, in the absence of irradiation; 2) under irradiation and in presence of precursor, bacterial inactivation was higher than that obtained with light alone. Such aspects indicate that the precursors at the considered concentration had no disinfecting/toxic effect on *E. coli* by themselves (i.e., in the dark)*,* and the tested lights effectively promote the transient species formation, accelerating bacterial inactivation. From Figure 1 it can be also noted that in the presence of precursors under irradiation, *E. coli* inactivation kinetics demonstrated an initial lag time followed by an exponential decay. This behavior has been widely reported for disinfection of both synthetic and real waters by SODIS (Giannakis et al., 2018; Giannakis et al., 2015; Ndounla et al., 2014, 2013; Sciacca et al., 2010).
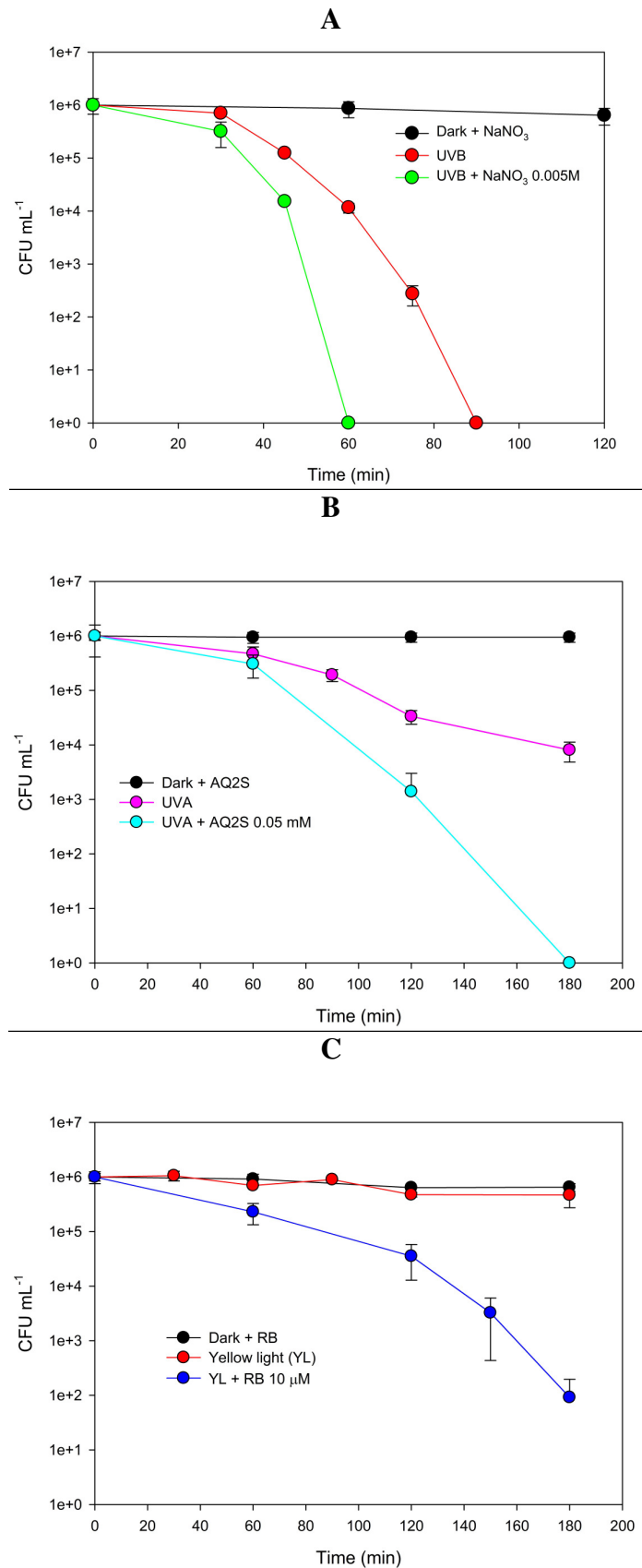
Figure 1. *E. coli* inactivation at various concentrations using the photosensitizers under irradiation. **A.** NaNO$_3$ and UVB light. **B.** AQ2S and UVA light. **C.** RB and yellow light (YL).

The photo-induced bacterial inactivation can involve internal and/or external pathways (Giannakis et al., 2018; Imlay, 2003). Since photo-generated $HO^{\bullet}$, $^1O_2$ and $^3AQ2S^*$ have a short lifetime (thus they can't cross the bacterial membrane and reach the internal cell components) and high reactivity with bacterial cell wall components, the damage they inflict when produced by extra-cellular precursors would be limited to the membrane itself. In other words, short-lived extracellular transient species kill bacteria (or at least impair their ability to replicate, as seen by colonies formation) by disrupting the cell membrane (Giannakis et al., 2018; Giannakis et al., 2016). However, the bacterial membrane can sustain a certain level of damage before rupture. Therefore, because a significant amount of damage is required to achieve bacterial death via membrane disruption, the phenomenon is reflected into the lag time A previous report mentions numbers up to 10^9 $HO^{\bullet}$ in order to inactivate 1 cell (Marugán et al., 2008).

After the lag phase, the exponential inactivation phase can be triggered (Giannakis et al., 2018; Giannakis et al., 2015). In the case of endogenous bacterial inactivation by irradiation alone, the lag time is caused by enzymatic DNA repair mechanisms that contrast, up to a certain degree, the DNA damage caused by UV photons (Rastogi et al., 2010). Hence, a complete kinetic analysis of the interaction of bacteria with $HO\bullet$, $^3AQ2S^*$ and $^1O_2$ should consider both lag phase and exponential decay.

3.2 Limitation of the competition kinetics method for a complete analysis of bacterial inactivation

The competition kinetics method has been applied to characterize the interaction of bacteria with $HO\bullet$, $^3AQ2S^*$ and $^1O_2$ (Text S2 and Serna-Galvis et al., 2018). However, the rate constants for *E. coli* inactivation can only be determined after the lag-phase has finished, which means that the first data point used to calculate the fitting curve of the exponential phase is not the time zero point (Figure S3). Therefore, the use of competition kinetics implies that the lag phase of bacterial

inactivation is completely ignored. This is a strong limitation for the modeling of solar disinfection, because the process comprises both the lag-phase and the exponential decay. Therefore, a different strategy is required to take the lag phase into account. Previous works on degradation of organic pollutants in water have shown a good fitting to a lag equation (Carena et al., 2017). Thus, an alternative option for the kinetic analysis of photo-induced bacteria inactivation consists in the fit of the experimental data to a lag-type equation having the following form (Eq. 1):

$$\frac{CFU_t}{CFU_o} = e^{-kt} \frac{e^{kL}}{1 + (e^{kL} - 1)e^{-kt}} \tag{1}$$

where CFU_t is the bacterial count at the time t, CFU_o the initial bacterial count, k the pseudo-first order rate constant of bacterial inactivation, and L the lag time.

Data fit of experimental results (taken from Figure 1) to Eq. 1 was tested and a good fit was found (depicted in Figure 2). Then, to understand how the photo-generated transient species affect both the lag times and the subsequent exponential inactivation phase of the bacteria, the concentrations of the experimental photosensitizers (i.e., $NaNO_3$, AQ2S and RB) were varied (Figure S4) and the values for L and k were determined (Table 1). It can be seen that by increasing the concentration of the experimental photosensitizers (i.e., $NaNO_3$, AQ2S and RB), one obtains a shorter lag time and faster decay thereafter.

In the system containing nitrate under irradiation, the main phenomena occurring in the exponential phase after the lag time are endogenous inactivation, and exogenous inactivation by $HO^\bullet$ (Serna-Galvis et al., 2018). By assuming that both processes independently follow pseudo-first order kinetics with respective rate constants k_{endo} and k_{exo}, one has $k = k_{endo} + k_{exo}$. The role of endogenous inactivation can be assessed in irradiation experiments of *E. coli* alone, without $NaNO_3$, which allows for the determination of k_{endo}.
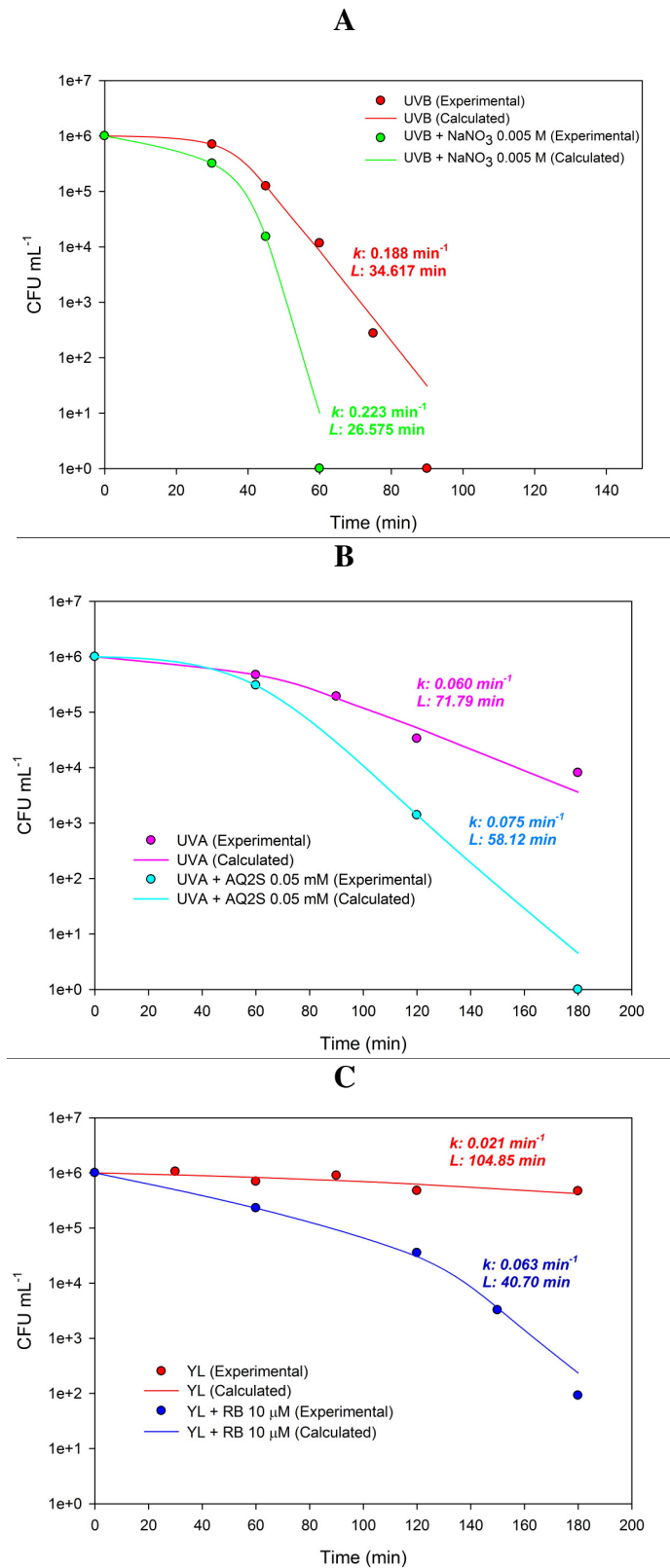
A

B

C

Figure 2. Evaluation of the experimental data fitting to Eq. 1.

Solid circles: Experimental values, *lines*: values calculated using Eq.1. Experimental data

were taken from Figure1.

Table 1. Estimated values for *L* and *k* from the experimental data (Figure S4).

Treatment system	k	L
UVB	0.118	34.62
UVB + NaNO$_3$ 0.005M	0.223	26.575
UVB + NaNO$_3$ 0.01M	0.478	18.334
UVA	0.060	71.79
UVA + AQ2S 0.01mM	0.064	67.17
UVA + AQ2S 0.05mM	0.075	58.12
YL	0.020	104.85
YL + RB 10 µM	0.063	40.70
YL + RB 100 µM	0.084	28.99

The value of k_{exo} depends on the reaction between HO$^\bullet$ and the bacteria, as $k_{exo} = k_{HO^\bullet}^{E.coli}$ [HO$^\bullet$], where $k_{HO^\bullet}^{E.coli}$ is the second-order inactivation rate constant of *E. coli* by HO$^\bullet$ (2.5×10^{11} L mol^{-1} s^{-1}; Serna-Galvis et al., 2018). Note that the diffusion-control limit in aqueous solution, which constitutes an upper limit for the second-order reaction rate constants, can be much higher than 10^{10} L mol^{-1} s^{-1} if the two reactive species have very different size, like $^\bullet$OH and a bacterium (Desmond-Le Quéméner and Bouchez, 2014). Therefore, k_{exo} measures the steady-state [HO$^\bullet$] in the irradiated system containing nitrate, and the experimental value of k, obtained upon application of Eq. 2, can be used to derive [HO$^\bullet$] after accounting for endogenous inactivation (i.e., [HO$^\bullet$] = (k - k_{endo}) $(k_{HO^\bullet}^{E.coli})^{-1}$). By so doing, one gets that in the experimental conditions of Figure S4A the steady-state [HO$^\bullet$] varies in the range of 10^{-14} - 10^{-13} mol L^{-1} as NaNO$_3$ varies from 0.005 to 0.05 mol L^{-1}. The

concentration of nitrate varies very slowly as the UVB irradiation progresses (Mack and Bolton, 1999), thus the [HO$^\bullet$] value found in the exponential decay phase can be considered as representative of the lag phase as well.

It is interesting to look for a correlation between the lag time and the steady-state [HO$^\bullet$], based on the assumption that the higher is [HO$^\bullet$], the faster the bacterial membrane is damaged and the shorter is the lag time as a consequence. However, irradiation itself also contributes to cell damage, and the irradiation of the bacteria without nitrate yields a lag time as well. In the case of the irradiation experiments in the presence of nitrate, one can make the simplified but reasonable assumption that the lag time is due to the action of two independent processes (radiation-endogenous and HO$^\bullet$-exogenous). The time L taken to reach the threshold (the loss of bacterial cell integrity) by the two processes acting together is lower than the times taken by the two processes acting separately (L_{endo} and L_{exo}, respectively). Therefore, the experimentally observed lag-time (L) can be expressed as follows (Eq. 2) (Hammes, 1978):

$$\frac{1}{L} = \frac{1}{L_{endo}} + \frac{1}{L_{exo}} \qquad (2)$$

The value of L_{endo} can be derived from the irradiation-alone experiments (without NaNO$_3$), and in our conditions a value of ~35 min was obtained. From Eq. (2) one can then derive the value of L_{exo}, and then study the effect of [HO$^\bullet$] on L_{exo}. The plot of L_{exo} vs. [HO$^\bullet$] (Figure 3) showed a decreasing trend that was phenomenologically well fitted with an exponential function ($r^2 = 0.996$) having the following form (Eq. 3):

$$L_{exo} = (158 \pm 10)\, e^{-((3.0 \pm 0.3) \times 10^{13})[HO^\bullet]} \qquad (3)$$

where L_{exo} is in minutes and [HO$^\bullet$] has units of M (mol L^{-1}). L_{exo} varied from 114 to 15 min as [HO$^\bullet$] varied between $(1-9) \times 10^{-14}$ mol L^{-1} (Figure 3).
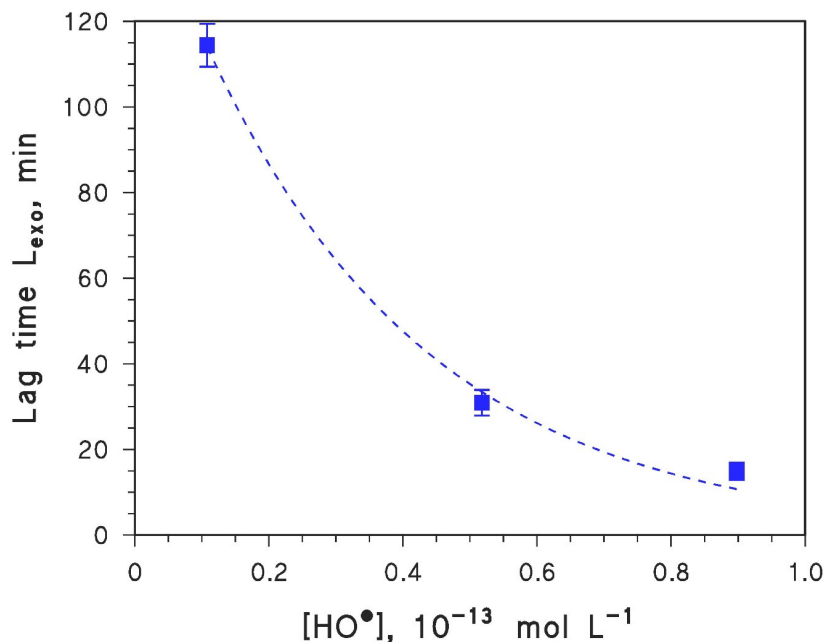
Figure 3. Plot of the lag time relevant for the exogenous inactivation of *E. coli* by HO˙, as a function of the steady-state [HO˙] under irradiation (see Eq. (3)). The latter was determined on the basis of the photoinactivation kinetics observed in the exponential phase, using the second-order inactivation rate constant of the bacteria by HO˙ (k_{exo} = $k_{HO˙}^{E.coli}$ [HO˙]).

Figure S4B presents the inactivation of *E. coli* under UVA irradiation only, with AQ2S in the dark, as well as under UVA in the presence of AQ2S at different concentrations. AQ2S in the dark (control experiment) showed no inactivation even after 180 min of contact time with the bacteria. UVA radiation alone induced a 2-log bacterial reduction in the studied time frame of 180 min, and the trend of the curve suggests that higher inactivation could be reached at longer irradiation times. On the other hand, the addition of AQ2S under irradiation significantly improved inactivation. In particular, 6-log inactivation could be reached in 120 min irradiation in the presence of 0.50 mM AQ2S. Both Table 1 and Figure S4B suggest that the lag time did not change much as [AQ2S] increased. Considering that the triplet state [3]AQ2S* is by far the main reactive species in irradiated AQ2S solutions (Bedini et al., 2012; Maddigapu et al., 2010), it can be inferred that [3]AQ2S* accelerated degradation by increasing k but had practically no effect on L. A possible, tentative

15

explanation for this behavior is that ^{3}AQ2S* is too bulky to reach cell-membrane sites where to make damage, differently from the much smaller HO$^\bullet$. In contrast, during the lag phase AQ2S may have time to enter the bacterial cell and there contribute to the acceleration of the exponential decay phase, through formation of intra-cellular ^{3}AQ2S*.

Figure S4C shows the inactivation trend of *E. coli* in the presence of Rose Bengal (RB) as $^1O_2$ source. First of all, the control experiment with RB in the dark showed that this compound is not toxic for bacteria. Moreover, no inactivation was caused by yellow light alone (~550 nm), which can be related to the low energy of this long-wavelength radiation. In contrast, significant inactivation was caused by the simultaneous occurrence of RB and yellow light, which is known to yield $^1O_2$ (Kellogg and Fridovich, 1975). For instance, a 5-log inactivation was found after 3 hours irradiation in the presence of 50 µM RB and, when doubling the RB concentration, the inactivation rate increased to achieve 6-log reduction after 2.5 hours (150 min).

By applying the same approach as in the case of HO$^\bullet$ (NaNO$_3$ irradiation), it was possible to assess the values of k_{exo} and L_{exo} that can be attributed to the action of $^1O_2$. Moreover, absence of inactivation by yellow light alone ensures that $k_{exo} \sim k$ and $L_{exo} \sim L$. Also in this case the bacteria can be used as $^1O_2$ probes in the irradiated solutions ($k_{exo} = k_{^1O_2}^{E.coli}$ [$^1O_2$] (Serna-Galvis et al., 2018)), and by so doing one obtains that L_{exo} values in the range of 65-40 min are associated to steady-state [$^1O_2$] in the range of $(0.7\text{-}1.0)\times10^{-10}$ mol L^{-1}. Interestingly, the steady-state [$^1O_2$] obtained here for 100 µmol L^{-1} RB (10^{-10} mol L^{-1}) is one order of magnitude higher compared to a previous study that used 10 µmol L^{-1} RB (i.e., 10 times lower compared to this study) under an otherwise similar irradiation set-up (De Laurentiis et al., 2014). $^1O_2$ can thus induce similar L_{exo} values as HO$^\bullet$, but with [$^1O_2$] $\sim 10^3$ [HO$^\bullet$]. Interestingly, this ratio runs in the opposite direction compared to the second-order reaction rate constants of $^1O_2$ and HO$^\bullet$ with *E. coli* ($k_{HO^\bullet}^{E.coli}$ ($k_{^1O_2}^{E.coli}$)$^{-1} \sim 10^4$, previous work, Serna-Galvis et al., 2018, and Table S2).

3.3 Implications for sunlit natural waters

In the previous sections it was shown that *E. coli* could be inactivated by $HO^\bullet$, $^1O_2$ and triplet states in an exponential way after a certain lag time. However, as far as the lag time itself is concerned, the triplet state $^3AQ2S^*$ played a negligible role. Considering that $^3AQ2S^*$ is usually more reactive than average $^3CDOM^*$ (Avetta et al., 2016), it can be reasonably assumed that the natural excited tripled states ($^3CDOM^*$) would not affect the bacterial lag time. The lag time could be modified in the presence of $HO^\bullet$ and $^1O_2$, and a comparable effect of the two species was observed for $[^1O_2] \sim 10^3\ [HO^\bullet]$. In sunlit natural waters one often has $[^1O_2] \gg [HO^\bullet]$ (Vione et al., 2014), but it is important to assess which $[^1O_2]\ [HO^\bullet]^{-1}$ ratios can be expected under different environmental conditions. In this way, one can see which of the two species is most likely to affect the lag time of the bacteria in the natural environment. To this purpose, photochemical modeling with the APEX software was carried out under different conditions of water depth and chemistry, with particular emphasis on DOC, nitrate and nitrite that are most likely to affect the steady-state $[HO^\bullet]$ and $[^1O_2]$ (Vione et al., 2014). The chosen conditions of sunlight irradiance were referred to the tropical belt (19°N, 15 July at noon) under clear sky, and the sunlight spectrum was obtained by means of the TUV software (National Center for Atmospheric Research, 2015). The choice of the latitude is motivated by the fact that bacteria photoinactivation is often exploited at the tropics, e.g., in the case of solar disinfection (SODIS) for water treatment (Fernàndez-Ibañez et al., 2017; Ndounla et al., 2014).

The simulation results are reported in Figure 4, under conditions of relatively high nitrate and nitrite (10^{-4} and 10^{-6} mol L^{-1}, respectively, Figure 4A) that tend to favor the $HO^\bullet$ occurrence, or with low nitrate and nitrite (10^{-6} and 10^{-8} mol L^{-1}, respectively, Figure 4B) that would in contrast favor $^1O_2$ processes at the expense of $HO^\bullet$ (Vione et al., 2014).

A

B

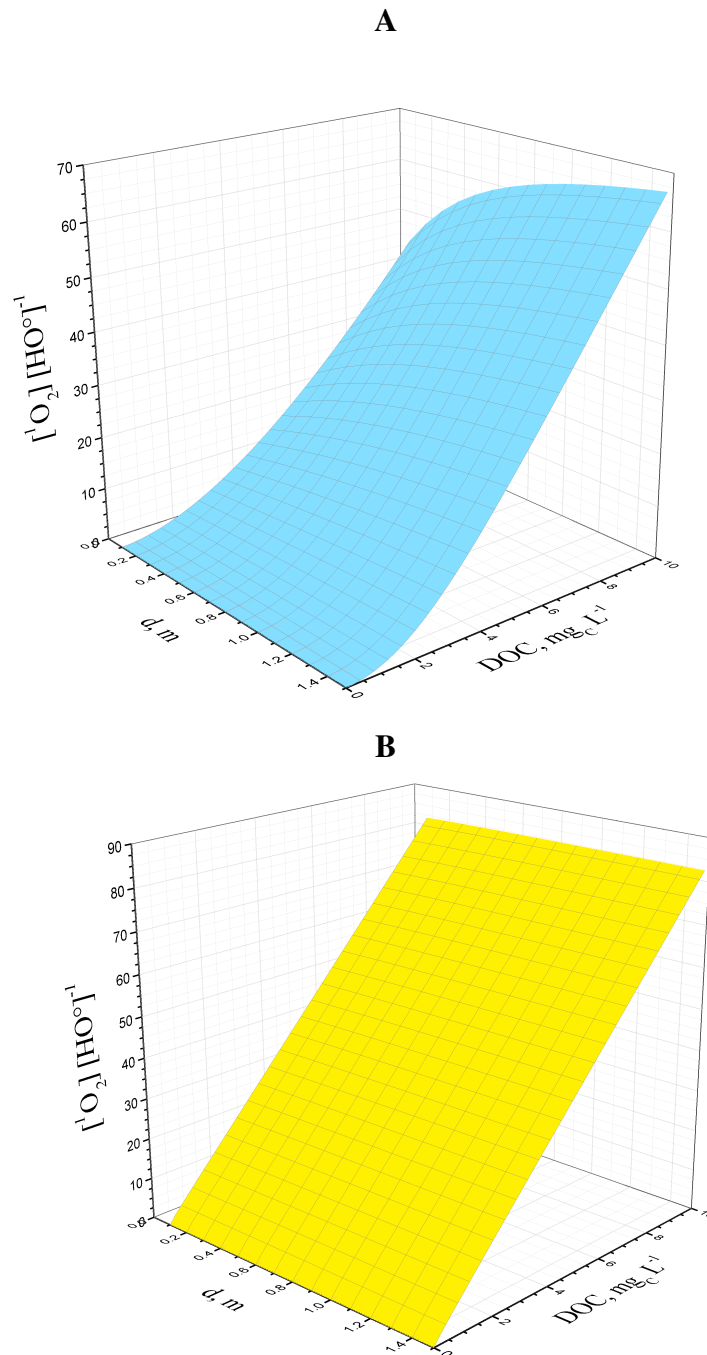**Figure 4.** APEX-simulated ratios of $[^1O_2]$ $[HO^\bullet]^{-1}$, as a function of water depth (d) and dissolved organic carbon (DOC), for sunlight irradiance conditions equivalent to tropical clear-sky summer (19°N, 15 July at noon). **A.** Other water conditions: 0.1 mM nitrate, 1 µM nitrite, 1 mM bicarbonate, 0.5 µM carbonate. **B.** Other water conditions: 1 µM nitrate, 10 nM nitrite, 1 mM bicarbonate, 0.5 µM carbonate.

The $[^1O_2]$ $[HO^\bullet]^{-1}$ ratio under the modeled conditions never exceeded 10^2. Although higher ratios could be obtained for DOC > 10 mg$_C$ L^{-1}, one would require unrealistically high DOC values to get $[^1O_2] \sim 10^3$ $[HO^\bullet]$, which is suggested by our experimental results to be the ratio where the two species comparably affect the bacterial lag time. The reported results were obtained by means of modeling, but there is evidence that the model reliability is high enough (Kohn et al., 2016) and the safety margin between 10^2 and 10^3 large enough to ensure the validity of the present conclusions. Moreover, experimental data obtained upon simulated-sunlight irradiation of lake water samples from temperate areas yielded $[^1O_2]$ $[HO^\bullet]^{-1} \sim 10^2$ (Vione et al., 2010), which is not far from our model results.

Therefore, because $[^1O_2] \sim 10^3$ $[HO^\bullet]$ is hardly attained in natural waters, one can conclude that the *E. coli* exogenous lag time in the natural environment would be mainly controlled by $HO^\bullet$. In the case of the exogenous inactivation of *E. coli*, an approach to model the exponential decay phase (which is accounted for by $^\bullet OH$, $^3CDOM*$ and $^1O_2$) after the lag time has already been developed in a previous publication (Serna-Galvis et al., 2018). Moreover, the $HO^\bullet$-affected lag time of exogenous inactivation is described by Eq. (3). Such an equation is just phenomenological, thus it is only valid in the same 10^{-14} mol L^{-1} $[HO^\bullet]$ range where it was obtained. Despite these limitations, the present approach allows for a complete modeling (lag time plus exponential phase) of the exogenous photoinactivation of *E. coli* under sunlight irradiation.

An example of the comparison between experimental irradiation data (*E. coli* inactivation by irradiated NaNO$_3$) and photochemical modeling based on Eqs. (1-3) is provided in Figure 5, showing a satisfactory agreement. To allow for comparison with actual experimental data, experimentally-derived endogenous inactivation kinetics was added to the modeled exogenous one to produce the predictive curves in the figure.

In order to obtain steady-state $[HO^\bullet]$ values around 10^{-14} mol L^{-1} in a real-world setting, we had to assume summertime and fair-weather tropical irradiation conditions (15 July, 19°N), high nitrate,

low DOC and low water depth. The APEX software was thus employed to search for suitable environmental conditions that provide $[HO^{\bullet}]$ in the range of 10^{-14} mol L^{-1}. Considering that solar disinfection can be used in tropical countries to obtain drinking water (Fernàndez-Ibañez et al., 2017; Ndounla et al., 2014), the chosen nitrate levels (up to 1 mM) were in the upper range of those still compatible with the WHO guidelines for drinking water quality (World Health Organization, 2017).
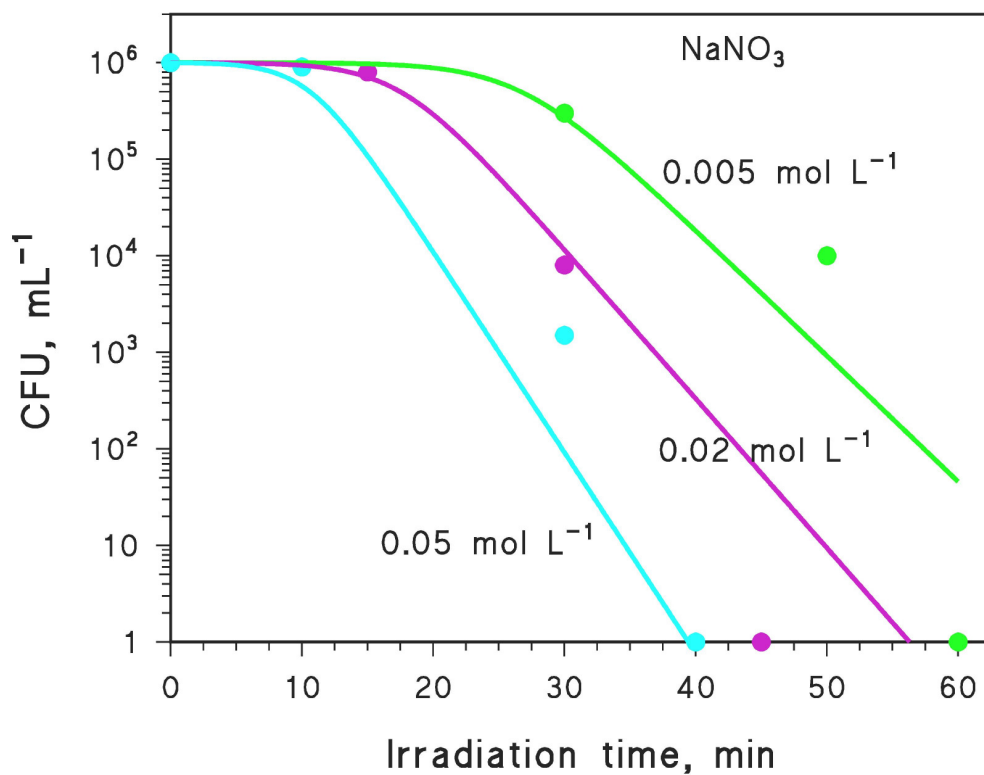

Figure 5. Comparison between the experimental data (solid circles) of bacteria photoinactivation upon UVB irradiation of $NaNO_3$ (see Figure S4A, with green = 0.005 M $NaNO_3$, purple = 0.02 M $NaNO_3$, and light blue = 0.05 M $NaNO_3$) and our model predictions (solid curves), based on Eqs. (2-4) in the main text. In particular, it was k_{endo} = 0.19 min^{-1}, L_{endo} = 34.6 min, $k_{exo} = k_{HO^{\bullet}}^{E.coli}$ $[HO^{\bullet}]$, and L_{exo} as per Eq. (3) in the main text.

Full photochemical modeling of bacterial inactivation should take the form of Eq. (1), thus there is the need to provide a model assessment of both the first-order inactivation rate constant k and the lag time L. The model determination of k can be made with the APEX software on the basis of sunlight irradiance, water chemistry, depth, as well as the *E. coli* inactivation rate constants with $HO^\bullet$, $^3CDOM^*$ and $^1O_2$, following a procedure that has been already described (Serna-Galvis et al., 2018). The assessment of L can be done with Eq. (3), provided that $[HO^\bullet]$ is not far from 10^{-14} mol L^{-1} levels.

An example of the results that can be obtained in this scenario is provided in Figure 6, where the complete inactivation curves are shown for different $[HO^\bullet]$ levels. The water conditions that produce the relevant $[HO^\bullet]$ values are given in the figure caption. With $[HO^\bullet] \sim 10^{-14}$ mol L^{-1}, the hydroxyl radical would largely control not only the lag time L, but also the inactivation rate constant k. The results reported in Figure 6 suggest a quite fast bacterial photo-inactivation, which would make the exogenous process competitive with the endogenous one. It should be stressed that these results were obtained by assuming specific water conditions (low depth, very low DOC, high nitrate). Low depth and low DOC are quite applicable to SODIS conditions because low water depth is prescribed in the guidelines of SODIS that suppose disinfection in PET or glass bottles (max 2 L volume, 10 cm diameter), while low DOC values are preferred for drinking water. Additionally, nitrate values in the high µM range are common, and even 1.2 mM nitrate is reported for water intended for human use (Ndounla et al., 2014).

Finally, it should be observed that the approach described here allowed us to fully model the exogenous bacterial photo-inactivation trend under natural-water conditions that are characterized by high $[HO^\bullet]$. In several real cases the steady-state $[HO^\bullet]$ would actually be lower (and sometimes much lower) than 10^{-14} mol L^{-1}. However, in such circumstances the $HO^\bullet$-induced rate constant of exponential inactivation would also be quite low and the $HO^\bullet$-associated lag time quite long, making bacterial inactivation by $HO^\bullet$ ineffective. Therefore, in the presence of low $[HO^\bullet]$ the

associated inactivation kinetics would be slow as compared with typical SODIS exposure times (Serna-Galvis et al., 2018), making the role of HO$^\bullet$ in bacterial inactivation negligible. Therefore, while on the one hand our approach strictly requires [HO$^\bullet$] in the range of 10^{-14} mol L^{-1} to fully model *E. coli* inactivation, on the other hand lower [HO$^\bullet$] levels would produce insignificant inactivation that is of limited interest for modeling. Moreover, to obtain [HO$^\bullet$] » 10^{-14} mol L^{-1} that is also outside our modeling range, one needs toxic nitrate concentration values that are not relevant to SODIS.
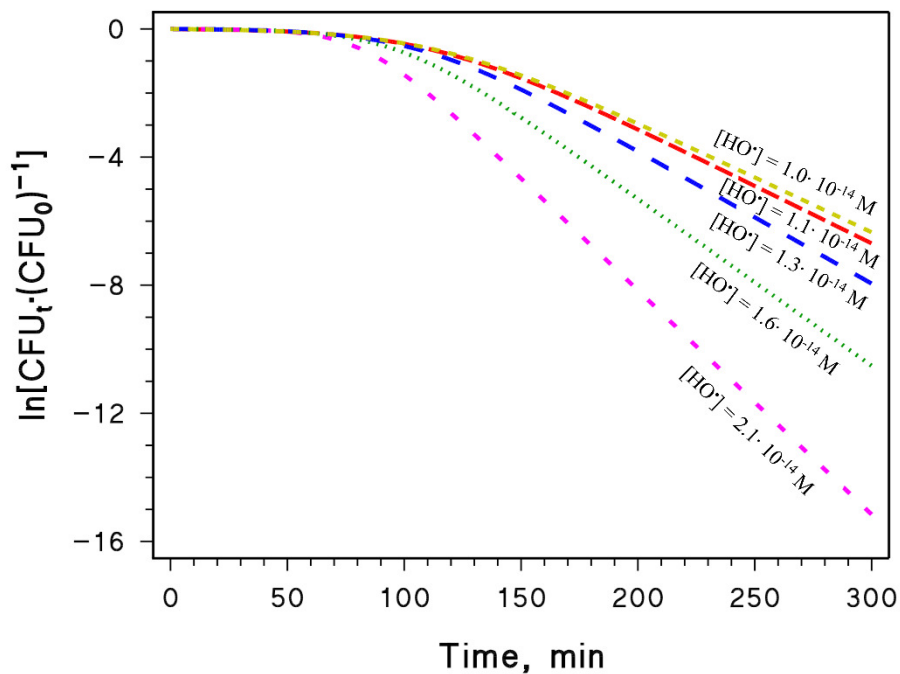

Figure 6. APEX-modeled exogenous photoinactivation of *E. coli* bacteria, as a function of the steady-state [HO$^\bullet$]. These curves are obtained with Eq. (1), using the modeled values for k and L. Different water conditions had to be chosen to obtain the reported [HO$^\bullet$] values, namely: $1.0 \cdot 10^{-14}$ M (1 mM NO$_3^-$, 0.4 mg$_C$ L^{-1} DOC); $1.1 \cdot 10^{-14}$ M (0.5 mM NO$_3^-$, 0.1 mg$_C$ L^{-1} DOC); $1.3 \cdot 10^{-14}$ M (1 mM NO$_3^-$, 0.3 mg$_C$ L^{-1} DOC); $1.6 \cdot 10^{-14}$ M (1 mM NO$_3^-$, 0.2 mg$_C$ L^{-1} DOC); $2.1 \cdot 10^{-14}$ M (1 mM NO$_3^-$, 0.1 mg$_C$ L^{-1} DOC). In all the case it was assumed 10 cm water depth, 1 mM HCO$_3^-$, 0.5 µM CO$_3^{2-}$, and 0.1 µM NO$_2^-$.

4. Conclusions

- The photoinduced *E. coli* inactivation has both lag and exponential decay phases, and a quantitative description of the system cannot be achieved by using competition kinetics alone, which only helps quantify the exponential phase.

- We showed that the lag time is mostly influenced by irradiation (endogenous inactivation) and $HO^\bullet$ (exogenous inactivation), while $^1O_2$ and triplet states only affect the exponential phase.

- The contribution of $HO^\bullet$ to the lag time L was phenomenologically well fitted with an exponential function that correlates L with the steady-state $[HO^\bullet]$. Unfortunately, this phenomenological equation works just in the 10^{-14} mol L^{-1} $[HO^\bullet]$ range where it was obtained, but we got evidence that only these steady-state concentration values are significant to SODIS. Indeed, APEX modeling of the exogenous photo-inactivation of *E. coli* suggests that lower $[HO^\bullet]$ would produce insignificant cell death, thus $HO^\bullet$ in such conditions would hardly affect either the lag or the exponential phase. On the other hand, much higher $[HO^\bullet]$ values are not significant to SODIS because they require excessively high nitrate levels that would be toxic for humans. Therefore, despite its limitations, our approach achieved the full modeling of exogenous photo-inactivation where it has chances to be significant. The next problem to be tackled in future works should be the full modeling of endogenous bacterial inactivation, with particular emphasis on the lag phase.

Acknowledgments

References

Avetta, P., Fabbri, D., Minella, M., Brigante, M., Maurino, V., Minero, C., Pazzi, M., Vione, D., 2016. Assessing the phototransformation of diclofenac, clofibric acid and naproxen in surface waters: Model predictions and comparison with field data. Water Res. 105, 383–394. https://doi.org/10.1016/j.watres.2016.08.058

Bedini, A., De Laurentiis, E., Sur, B., Maurino, V., Minero, C., Brigante, M., Mailhot, G., Vione, D., 2012. Phototransformation of anthraquinone-2-sulphonate in aqueous solution. Photochem. Photobiol. Sci. 11, 1445–1453. https://doi.org/10.1039/C2PP25111F

Bodrato, M., Vione, D., 2014. APEX (Aqueous Photochemistry of Environmentally occurring Xenobiotics): a free software tool to predict the kinetics of photochemical processes in surface waters. Environ. Sci. Process. Impacts 16, 732–740. https://doi.org/10.1039/C3EM00541K

Braslavsky, S.E., 2007. Glossary of terms used in photochemistry, 3rd edition (IUPAC Recommendations 2006). Pure Appl. Chem. 79, 293–465. https://doi.org/10.1351/pac200779030293

Carena, L., Minella, M., Barsotti, F., Brigante, M., Milan, M., Ferrero, A., Berto, S., Minero, C., Vione, D., 2017. Phototransformation of the Herbicide Propanil in Paddy Field Water. Environ. Sci. Technol. 51, 2695–2704. https://doi.org/10.1021/acs.est.6b05053

Cory, R.M., McKnight, D.M., 2005. Fluorescence spectroscopy reveals ubiquitous presence of oxidized and reduced quinones in dissolved organic matter. Environ. Sci. Technol. 39, 8142–8149. https://doi.org/10.1021/es0506962

Davies-Colley, R.J., Donnison, A.M., Speed, D.J., 2000. Towards a mechanistic understanding of paleoproxies. Water Sci. Technol. 42, 149–158.

De Laurentiis, E., Prasse, C., Ternes, T.A., Minella, M., Maurino, V., Minero, C., Sarakha, M., Brigante, M., Vione, D., 2014. Assessing the photochemical transformation pathways of

acetaminophen relevant to surface waters: Transformation kinetics, intermediates, and modelling. Water Res. 53, 235–248. https://doi.org/10.1016/j.watres.2014.01.016

Desmond-Le Quéméner, E., Bouchez, T., 2014. A thermodynamic theory of microbial growth. ISME J. 8, 1747-1751. https://doi.org/10.1038/ismej.2014.7.

Fernàndez-Ibañez, P., McGuigan, K.G., Fatta-Kassinos, D., 2017. Can solar water-treatment really help in the fight against water shortages? Europhys. News 48, 26–30. https://doi.org/10.1051/epn/2017304

Giannakis, S., 2018. Analogies and differences among bacterial and viral disinfection by the photo-Fenton process at neutral pH: a mini review. Environ. Sci. Pollut. Res. https://doi.org/10.1007/s11356-017-0926-x

Giannakis, S., Darakas, E., Escalas-Cañellas, A., Pulgarin, C., 2015. Solar disinfection modeling and post-irradiation response of Escherichia coli in wastewater. Chem. Eng. J. 281, 588–598. https://doi.org/10.1016/j.cej.2015.06.077

Giannakis, S., Darakas, E., Escalas-Cañellas, A., Pulgarin, C., 2015. Environmental considerations on solar disinfection of wastewater and the subsequent bacterial (re)growth. Photochem. Photobiol. Sci. 14. https://doi.org/10.1039/c4pp00266k

Giannakis, S., Polo López, M.I., Spuhler, D., Sánchez Pérez, J.A., Fernández Ibáñez, P., Pulgarin, C., 2016. Solar disinfection is an augmentable, in situ-generated photo-Fenton reaction—Part 1: A review of the mechanisms and the fundamental aspects of the process. Appl. Catal. B Environ. 199, 199–223. https://doi.org/10.1016/j.apcatb.2016.06.009

Giannakis, S., Ruales-Lonfat, C., Rtimi, S., Thabet, S., Cotton, P., Pulgarin, C., 2016. Castles fall from inside: Evidence for dominant internal photo-catalytic mechanisms during treatment of Saccharomyces cerevisiae by photo-Fenton at near-neutral pH. Appl. Catal. B Environ. 185. https://doi.org/10.1016/j.apcatb.2015.12.016

Giannakis, S., Voumard, M., Rtimi, S., Pulgarin, C., 2018. Bacterial disinfection by the photo-Fenton process: Extracellular oxidation or intracellular photo-catalysis? Appl. Catal. B Environ. 227, 285–295. https://doi.org/https://doi.org/10.1016/j.apcatb.2018.01.044

Hammes, G., 1978. Principles of Chemical Kinetics, First Edit. ed. Academic Press, New York.

Imlay, J.A., 2003. Pathways of oxidative damage. Annu. Rev. Microbiol. 57, 395–418.

Kellogg, E.W., Fridovich, I., 1975. Superoxide, Hydrogen Peroxide, and Singlet Oxygen in Lipid Peroxidation by a Xanthine Oxidase System*. J. Biol. Chem. 250, 8812–8817.

Kochevar, I.E., Redmond, R.W., 2000. Photosensitized production of single oxygen. Methods Enzymol. 319, 20–28. https://doi.org/10.1016/S0076-6879(00)19004-4

Kohn, T., Mattle, M.J., Minella, M., Vione, D., 2016. A modeling approach to estimate the solar disinfection of viral indicator organisms in waste stabilization ponds and surface waters. Water Res. 88, 912–922. https://doi.org/10.1016/j.watres.2015.11.022

Loeff, I., Treinin, A., Linschitz, H., 1984. The photochemistry of 9,10-anthraquinone-2-sulfonate in solution. 2. Effects of inorganic anions: quenching vs. radical formation at moderate and high anion concentrations. J. Phys. Chem. 88, 4931–4937. https://doi.org/10.1021/j150665a028

Loiselle, S.A., Azza, N., Cozar, A., Bracchini, L., Tognazzi, A., Dattilo, A., Rossi, C., 2008. Variability in factors causing light attenuation in Lake Victoria. Freshw. Biol. 53, 535–545. https://doi.org/10.1111/j.1365-2427.2007.01918.x

Mack, J., Bolton, J.R., 1999. Photochemistry of nitrite and nitrate in aqueous solution: a review. J. Photochem. Photobiol. A Chem. 128, 1. https://doi.org/http://dx.doi.org/10.1016/S1010-6030(99)00155-0

Maddigapu, P.R., Bedini, A., Minero, C., Maurino, V., Vione, D., Brigante, M., Mailhot, G., Sarakha, M., 2010. The pH-dependent photochemistry of anthraquinone-2-sulfonate. Photochem. Photobiol. Sci. 9, 323. https://doi.org/10.1039/b9pp00103d

Maraccini, P.A., Wenk, J., Boehm, A.B., 2016. Exogenous indirect photoinactivation of bacterial pathogens and indicators in water with natural and synthetic photosensitizers in simulated sunlight with reduced UVB. J Appl Microbiol 121, 587–597. https://doi.org/10.1111/jam.13183

Marugán, J., van Grieken, R., Sordo, C., Cruz, C., 2008. Kinetics of the photocatalytic disinfection of Escherichia coli suspensions. Appl. Catal. B Environ. 82, 27–36. https://doi.org/http://dx.doi.org/10.1016/j.apcatb.2008.01.002

McGuigan, K.G., Conroy, R.M., Mosler, H.J., du Preez, M., Ubomba-Jaswa, E., Fernandez-Ibañez, P., 2012. Solar water disinfection (SODIS): A review from bench-top to roof-top. J. Hazard. Mater. 235–236, 29–46. https://doi.org/10.1016/j.jhazmat.2012.07.053

Minella, M., Giannakis, S., Mazzavillani, A., Maurino, V., Minero, C., Vione, D., 2017. Phototransformation of Acesulfame K in surface waters: Comparison of two techniques for the measurement of the second-order rate constants of indirect photodegradation, and modelling of photoreaction kinetics. Chemosphere 186. https://doi.org/10.1016/j.chemosphere.2017.07.128

National Center for Atmospheric Research, 2015. Quick TUV Calculator [WWW Document].

Ndounla, J., Kenfack, S., Wéthé, J., Pulgarin, C., 2014. Relevant impact of irradiance (vs. dose) and evolution of pH and mineral nitrogen compounds during natural water disinfection by photo-Fenton in a solar CPC reactor. Appl. Catal. B Environ. 148–149, 144–153. https://doi.org/http://dx.doi.org/10.1016/j.apcatb.2013.10.048

Ndounla, J., Spuhler, D., Kenfack, S., Wéthé, J., Pulgarin, C., 2013. Inactivation by solar photo-Fenton in pet bottles of wild enteric bacteria of natural well water: Absence of re-growth after one week of subsequent storage. Appl. Catal. B Environ. 129, 309–317. https://doi.org/10.1016/j.apcatb.2012.09.016

Nelson, K.L., Boehm, A.B., Davies-Colley, R.J., Dodd, M.C., Kohn, T., Linden, K.G., Liu, Y.,

Maraccini, P.A., McNeill, K., Mitch, W.A., 2018. Sunlight-mediated inactivation of health-relevant microorganisms in water: a review of mechanisms and modeling approaches. Environ. Sci. Process. Impacts 20, 1089–1122.

Onstein, P., Stefen, I.M., Bolton, J.R., 1999. Competition kinetics method for the determination of rate constants for the reaction of hydroxyl radicals with organic pollutants. J. Adv. Technol. 4, 231–236.

Rastogi, R.P., Kumar, A., Tyagi, M.B., Sinha, R.P., 2010. Molecular mechanisms of ultraviolet radiation-induced DNA damage and repair. J. Nucleic Acids 2010.

Rosario-Ortiz, F.L., Canonica, S., 2016. Probe Compounds to Assess the Photochemical Activity of Dissolved Organic Matter. Environ. Sci. Technol. 50, 12532–12547. https://doi.org/10.1021/acs.est.6b02776

Sciacca, F., Rengifo-Herrera, J.A., Wéthé, J., Pulgarin, C., 2010. Dramatic enhancement of solar disinfection (SODIS) of wild Salmonella sp. in PET bottles by H_2O_2 addition on natural water of Burkina Faso containing dissolved iron. Chemosphere 78, 1186–1191.

Serna-Galvis, E.A., Troyon, J.A., Giannakis, S., Torres-Palma, R.A., Minero, C., Vione, D., Pulgarin, C., 2018. Photoinduced disinfection in sunlit natural waters : Measurement of the second order inactivation rate constants between E . coli and photogenerated transient species. Water Res. 147, 242–253. https://doi.org/10.1016/j.watres.2018.10.011

Spuhler, D., Rengifo-Herrera, J., Pulgarín, C., 2010. Environmental The effect of Fe^{2+}, Fe^{3+}, H_2O_2 and the photo-Fenton reagent at near neutral pH on the solar disinfection (SODIS) at low temperatures of water containing Escherichia coli K12. Appl. Catal. B Environ. 96, 126–141. https://doi.org/10.1016/j.apcatb.2010.02.010

Vione, D., Bagnus, D., Maurino, V., Minero, C., 2010. Quantification of singlet oxygen and hydroxyl radicals upon UV irradiation of surface water. Environ. Chem. Lett. 8, 193–198.

https://doi.org/10.1007/s10311-009-0208-z

Vione, D., Falletti, G., Maurino, V., Minero, C., Pelizzetti, E., Malandrino, M., Ajassa, R., Olariu, R.-I., Arsene, C., 2006. Sources and Sinks of Hydroxyl Radicals upon Irradiation of Natural Water Samples. Environ. Sci. Technol. 40, 3775–3781. https://doi.org/10.1021/es052206b

Vione, D., Minella, M., Maurino, V., Minero, C., 2014. Indirect Photochemistry in Sunlit Surface Waters: Photoinduced Production of Reactive Transient Species. Chem. – A Eur. J. 20, 10590–10606. https://doi.org/10.1002/chem.201400413

World Health Organization, 2017. Guidelines for drinking-water quality. https://doi.org/10.1016/S1462-0758(00)00006-6